Metrol. Meas. Syst., Vol. 24 (2017), No. 4, pp. 631–644.

PAN POLSKA AKADEMIA NAUK

METROLOGY AND MEASUREMENT SYSTEMS

Index 330930, ISSN 0860-8229

www.metrology.pg.gda.pl

M&MS

LEAK DETECTION IN WATERWORKS: COMPARISON BETWEEN STFT AND FFT WITH AN OVERCOMING OF LIMITATIONS

Aimé Lay-Ekuakille[1)], Giuseppe Griffo[1)], Paolo Visconti[1)], Patrizio Primiceri[1)], Ramiro Velazquez[2)]

1) University of Salento, Department of Innovation Engineering, Via Monteroni, 73100 Lecce, Italy (✉ aime.lay.ekuakille@unisalento.it, +39. 0832 297 821 822, giuseppe.griffo@unisalento.it, paolo.visconti@unisalento.it, patrizio.primiceri@unisalento.it)

2) Panamerican University, Faculty of Engineering, Av. Josemaría Escrivá de Balaguer 101, 20290 Aguascalientes, Mexico (rvelazquez@ags.up.mx)

Abstract

Detection of leakages in pipelines is a matter of continuous research because of the basic importance for a waterworks system is finding the point of the pipeline where a leak is located and – in some cases – a nature of the leak. There are specific difficulties in finding leaks by using spectral analysis techniques like FFT (*Fast Fourier Transform*), STFT (*Short Term Fourier Transform*), *etc*. These difficulties arise especially in complicated pipeline configurations, *e.g.* a zigzag one. This research focuses on the results of a new algorithm based on FFT and comparing them with a developed STFT technique. Even if other techniques are used, they are costly and difficult to be managed. Moreover, a constraint in the leak detection is the pipeline diameter because it influences accuracy of the adopted algorithm. FFT and STFT are not fully adequate for complex configurations dealt with in this paper, since they produce ill-posed problems with an increasing uncertainty. Therefore, an improved Tikhonov technique has been implemented to reinforce FFT and STFT for complex configurations of pipelines. Hence, the proposed algorithm overcomes the aforementioned difficulties due to applying a linear algebraic approach.

Keywords: uncertainty, measurements, magnetic sensors, leak detection in pipelines, regularization.

1. Introduction

Spectral analysis techniques have stimulated great interest in the fields of measurements and sensing systems. They are simple to apply and belong to software techniques based on computations as opposed to the hardware ones based on dedicated instrumentation. In this paper, we implement FFT and STFT algorithms, which is an obvious but not trivial approach when applied to a zigzag hydraulic circuit representing a complicated case-study since, in many cases, we do not refer to this kind of configuration but it is possible to find it in industrial applications. Leak detection in pipelines and waterworks has an economic impact on a budget of public and private company managing such services. Quality of water is associated with environment protection because of possible intrusion of pollution in pipelines and diminishing of water quality with pollution of aquifers. Leaks are considered as small pressure discontinuities in the original pressure trace and increase the damping of the overall pressure signal [1]. Such partial reflections divert energy away from the main waveform and increase the decay rate of the transient signal. The behaviour of this pressure trace is, therefore, an indication of leaks within the system and can be used as a means of leak detection. To be practical, some examples can be given; those that use: (i) inverse methods to determine parameters in transient models by comparison with observed data (inverse transient analysis), (ii) transient damping-free-vibrational analysis, and also (iii) methods that use the time of arrival and magnitude of leak-reflected signals in order to determine leak location. The

Article history: received on Mar. 11, 2016; accepted on Aug. 23, 2017; available online on Dec. 01, 2017; DOI: 10.1515/mms-2017-0049.

subsequent pressure response due to leakage is measured and analysed to derive useful system information. The above approach is generally known as system response extraction and forms the main aspects of well-established methodologies. They are used to extract dynamic responses [2] of complex mechanical and electrical systems. Diverse spectral techniques, more robust than STFT and FFT have been implemented. Among them, we recall FDM (*Filter Diagonalization Method*), DSD (*Decimated Signal Diagonalization*) and DPA (*Decimated Padé Approximant*). FDM is a robust technique capable of avoiding the influence of noise for huge signals to be processed [3, 4]. DSD is still robust but fast and more accurate than FDM for a portion of signals to be treated [5] while DPA is a specific case of processing able to implement fast approximation with a powerful quickness [6]. All three techniques are suitable to convert nonlinearities into linear items, exploiting the linear algebra.

For small transient signals, the impact of nonlinearity in pipeline systems is negligible and, for these cases, a pipeline can be considered as a linear system. Whereas resonance frequencies reinforce and transmit input signals, other frequencies are absorbed within the system [7]. In this respect, pipeline systems are similar to frequency filters, the characteristics of which are determined by system properties such as boundary conditions, friction, and wave speed. Using the convolution theorem regarding the Fourier Transform, it is possible to define an inverse signal in respect to convolution. Suppose that we have a signal g and we would like to find a signal (if it exists) g^{-1} with the property that $g * g^{-1} = \delta$, in which " * " is intended as a cross product. The transform of a δ function (Kronecker in discrete time and Dirac in continuous time) is just a constant 1.

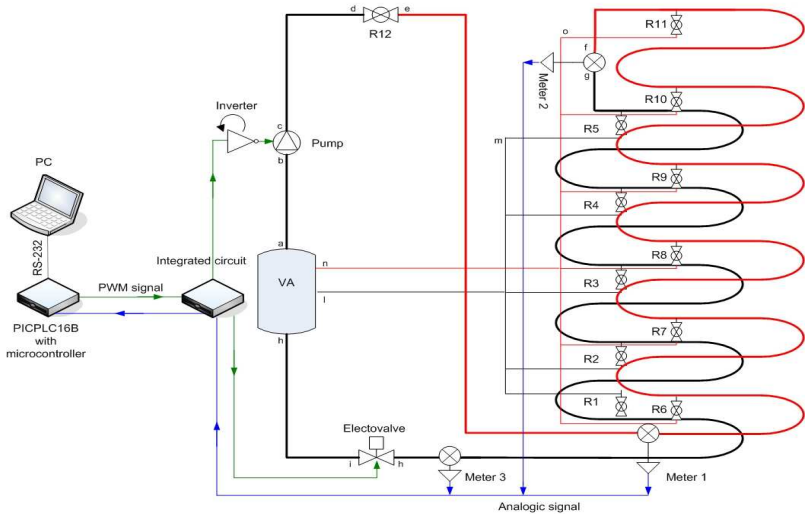

Fig. 1. Hydraulic and acquisition architectures of a pipeline hung on the lab wall.

The created hydraulic system uses a special zigzag pipeline simulating an experimental and complex waterworks 120 meters long and with a diameter of 1 inch. It is made of copper coated with a plastic film. It contains 11 water taps located on the pipeline and 3 magnetic sensors. A dedicated electronic architecture has been implemented for acquiring and processing signals produced by the magnetic sensors. A scheme of the architecture is shown in Fig. 1, whereas its photo – in Fig. 2. The system is hung on a vertical wall of the laboratory of Measurement and Instrumentation of the Department of Innovation Engineering – University of Salento, Italy. The fundamental interest, as announced before, is in trying to use the STFT and FFT techniques,

which – even if not robust for the purpose of the research can be employed thanks to some improvements, *e.g.* a further demonstrated *ad hoc* solution to ill-posed problems using an *L*-curve approach.

The experimental activities have been carried out starting with the regulation of water taps (see Fig. 3) to understand the effects on the water trends within the pipeline. A reservoir shown in Fig. 2 serves for storing approximately 100 litres of water used for filling the pipeline.

Fig. 2. A photo of the experimental system hung on a lab wall.

Actually, the pipeline has two parts, the first being an old circuit constructed with 6 water taps and one magnetic transducer. To make it more complex, a second part was added including 5 new water taps (Fig. 3), and it was superimposed to the first part. This is a stressing configuration, very complex for experimental activities. Both previous and new portions have a certain influence on leak position recovery as will be seen in the results' section.

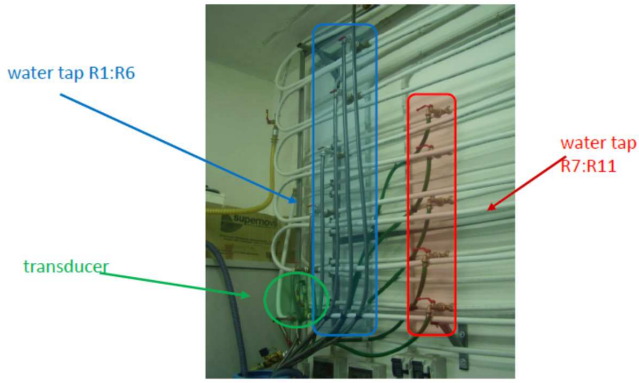

Fig. 3. A zoomed view of all water taps simulating leaks.

Even so we have experimented with other techniques on the same hydraulic circuit, we report the calibration that leads to a correlation between peak and opening/closing manoeuvers of water taps. That is an essential procedure on the proviso that the right peak should be found. The valve or water tap status and its duration enable to determine the trend at a certain pressure produced by the pump. Pressure fluctuations are studied for any water tap as shown in Fig. 4, in order to understand the eventual clutter pressure. For the cases under test, the pump delivers water at the same pressure in order to simulate a real waterworks. That is carried out thanks to a specially implemented electronic control.

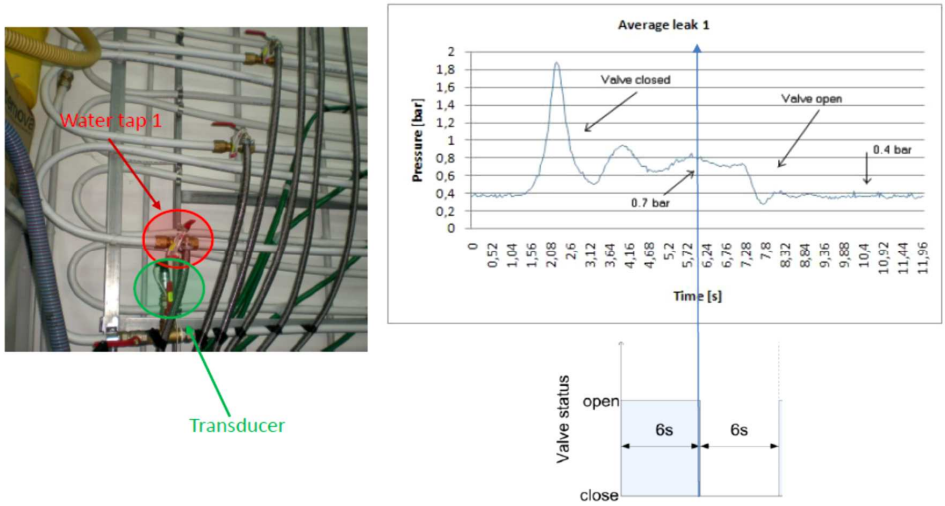

Fig. 4. Trials for calibrating the system and for detecting leaks by opening and closing a water tap.

2. STFT approach

The STFT represents a sort of compromise between the time- and frequency-based views of a signal. It provides some information about both when and at what frequencies a signal event occurs. However, we can only obtain this information with a limited precision and such a precision is determined by the size of the window. As described in Section 1, vibrations are created during leak, and using an electronic instrument or a proper sensing device it is possible to convert them in sounds or – equivalently – in the sum of sinusoids. So, the spectral responses are characterized by spectrograms that are produced by a procedure known as the *Short-Time Fourier Transform* (STFT). The STFT divides the entire signal into a series of successive short-time segments, called *records* (or *frames*). Each record is used as an input to the *Discrete Fourier Transform* (DFT), generating a series of spectra (one for each record).

Let $(X(t))_{t\in Z}$ be a digital signal. We review here the conditions for perfect reconstruction of the signal through STFT and inverse STFT [8]. Let N be a window length, R a window shift, W an analysis window function and S a synthesis window function. We assume that W and S are zero outside an interval $0 \le t \le N-1$. Also, we assume that the window length N is an integer multiple of the shift R and we note $Q = N/R$. The STFT for frame m is defined as the DFT of the windowed short-time signal $W(t - mR)\, X(t)$ (with the phase origin at the start of the frame, $t = mR$). The inverse STFT procedure consists in Fourier-inverting of each frame of the STFT spectrogram, multiplying each obtained (periodic) short-time signal by a synthesis window and summing together all the windowed short-time signals. In a particular frame $mR \le t \le mR+N-1$, which leads to a reconstructed signal $Y(t)$ given by:

$$\begin{aligned} Y(t) &= S(t - mR)\, W(t - mR)\, X(t) \\ &+ \sum_{q=1}^{Q-1} S(t - m(m-q)R)\, W(t - (m-q)R)\, X(t) \\ &+ \sum_{q=1}^{Q-1} S(t - m(m+q)R)\, W(t - (m+q)R)\, X(t)\,, \end{aligned} \tag{1}$$

where the three terms on the right-hand side are respectively a contribution of the inverse transforms of frame m, overlapping frames on the left and overlapping frames on the right. As

the contributions of frames with an index difference larger than Q do not overlap, by equating $Y(t) = X(t)$ for all t, we obtain as in [9] the following necessary condition for perfect reconstruction:

$$1 = \sum_{q=0}^{Q-1} W(t - qR)S(t - qR). \tag{2}$$

3. Implemented FFT and STFT algorithms for spectral analysis

With $|\cdot)$ we denote a representation of vectors in a vector space H; given two vectors $|a), |b) \in H$ the notation $(\cdot|\cdot)$ indicates a complex symmetric inner product such as $(a|b) = (b|a)$. During computation of this product, we only carried out transposition but not the complex conjugate. For example, given the following vectors: $|a) = \begin{bmatrix} j & 1-j \end{bmatrix}^T$ and $|b) = \begin{bmatrix} 2j & 1 \end{bmatrix}^T$ we have:

$$(a|b) = (b|a) = \begin{bmatrix} j & 1-j \end{bmatrix} \begin{bmatrix} 2j \\ 1 \end{bmatrix} = \begin{bmatrix} 2j & 1 \end{bmatrix} \begin{bmatrix} j \\ 1-j \end{bmatrix} = -1 - j. \tag{3}$$

We identify a linear operator on the vector space H with a superscript $\hat{}$, *e.g.* $\hat{U}, \hat{\Omega}$, *etc*. To indicate the application of an operator to a vector, we denote $|b) = \hat{\Omega}|a)$. An operator is defined diagonalisable if it is itself a set of eigenvalues ω_k and eigenvectors $|\omega_k)$ such as :

$$\hat{\Omega}|\omega_k) = \omega_k|\omega_k), \tag{4}$$

where the eigenvectors are orthonormalized in respect to the complex symmetric inner product:

$$(\omega_k|\omega_{k'}) = \delta_{kk'}. \tag{5}$$

When the eigenvectors $|\omega_k)$ constitute a complete basis, for the operator identity it is:

$$\hat{I} = \sum_k |\omega_k)(\omega_k|. \tag{6}$$

That implies that we can write $\hat{\Omega}$ by means of its spectral representation:

$$\hat{\Omega} = \sum_k \omega_k |\omega_k)(\omega_k|. \tag{7}$$

A spectral representation is useful when it is necessary to obtain information from a spectral function $f(\hat{\Omega})$ of operator $\hat{\Omega}$ for which eigenvalues and eigenvectors are known:

$$f(\hat{\Omega}) = \sum_k f(\omega_k)|\omega_k)(\omega_k|. \tag{8}$$

The function $f(\hat{\Omega})$ is also an operator, with eigenvalues $f(\omega_k)$ and eigenvectors $|\omega_k)$. In terms of quantum mechanics, since we deal with vibrations within the pipelines, if $\hat{\Omega}$ identifies an operator which is linear, hamiltonian and symmetric, with eigenvalues ω_k and eigenvectors $|\omega_k)$, it will be of great importance to use the associated temporal evolution operator: $\hat{U} = e^{-j\hat{\Omega}t}$. In fact, if $|0)$ is the system initial state, a state $|t)$ at a moment t is given by:

$$|t) = \hat{U}(t)|0). \tag{9}$$

The time-dependent autocorrelation functionis then given by:

$$\xi(t) = (0 \mid t) = (0 \mid \hat{U}(t) \mid 0) = (0 \mid e^{-j\hat{\Omega}t} \mid 0). \tag{10}$$

According to (8),the spectral representation $\hat{U}$ becomes:

$$\hat{U}(t) = f(\hat{\Omega}) = e^{-it\hat{\Omega}} = \sum_k e^{-it\omega_k} \mid \omega_k)(\omega_k \mid. \tag{11}$$

To show how the algorithm works, it is necessary to modify the FFT algorithm by defining a complex one-dimensional signal in the time domain, $c_n = C(t_n)$, defined in a set of equidistant time intervals $t_n = n\tau$, $n = 0,1,...,N-1$ as the sum of damped sinusoids:

$$c_n = \sum_{k=1}^{K} d_k e^{-in\tau\omega_k} = \sum_{k=1}^{K} d_k e^{-in\tau(2\pi f_k - i\gamma_k)} \tag{12}$$

with a total of 2*K* unknowns, that are *K* complex amplitudes d_s and *K* complex frequencies $\omega_k = 2\pi f_k - i\gamma_k$ that also include damping. Although (4) is nonlinear, its solution can be obtained with linear algebraic methods. The proposed FFT [12] associates an autocorrelation function, in an appropriate dynamic time system described by a complex Hamiltonian operator $\hat{\Omega}$ with complex eigenvalues $\{\omega_k\}$, with a signal c_n to be transformed in the form of (8):

$$c_n = \left(\Phi_0 \middle| e^{-in\tau\hat{\Omega}} \Phi_0\right). \tag{13}$$

In this way, the problem can be reduced to diagonalization of the Hamiltonian operator $\hat{\Omega}$ or, similarly, the evolution operator $\hat{U} = \exp(-i\tau\Omega)$.

A complex inner symmetric product operation is used in (13), namely $(a|b) = (b|a)$ without a complex conjugation, and Φ_0 is the initial state. Again, the symbol (.|.) denotes a complex symmetric inner product. Assuming we have a set of orthonormal eigenvectors $\{Y_k\}$ that diagonalize the evolution operator, we can clarify it as:

$$\hat{U} = \sum_k u_k \left|Y_k\right)(Y_k\right| = \sum_k \exp(-i\omega_k\tau) \left|Y_k\right)(Y_k\right| \tag{14}$$

and substituting (14) in (13), remembering to let:

$$d_k = (\Phi_0 \left|Y_k\right)(Y_k \left|\psi_0\right) = (Y_k \left|\Phi_0\right)^2. \tag{15}$$

The computed eigenvalues determine the positions of spectrum lines and their widths while the eigenvectors define their amplitudes and phases. Let us adopt a simple set created from Krylov vectors [11], generated by the evolution operator: $\Phi_n = \hat{U}^n \Phi_0 = \exp(-in\tau\hat{\Omega})\Phi_0$. According to (7), it gives:

$$(\Phi_n \left|\hat{U}\Phi_m\right.) = (\Phi_n \left|\Phi_{m+1}\right.) = c_{m+n+1}, \tag{16}$$

but since the set is not orthonormal, and we define a subspace of Krylov vectors generated by vectors of ***Q***, *i.e.* $Q = \{|0),|1),\ldots,|M-1)\}$, the overlap matrix should be computed as follows:

$$(\Phi_n \left|\Phi_m\right.) = (\hat{U}^n \Phi_0 \left|\hat{U}^m \Phi_0\right.) = (\Phi_0 \left|\hat{U}^{m+n} \Phi_0\right.) = c_{m+n+1}. \tag{17}$$

Therefore, it is strictly related to the values of measured signal. Then the following notation could be used: $\boldsymbol{U}^0$ is a representation of the (*M*+1) *x* (*M*+1) overlap matrix, similarly $\boldsymbol{U}^1$ is for $\hat{U}$. To signalize the formulation of (12), one must solve the generalized problem of eigenvalues, *i.e.*:

$$\mathbf{U}^1 \mathbf{B}_k = u_k \mathbf{U}^0 \mathbf{B}_k, \tag{18}$$

in which $u_k = \exp(-in\omega_k\tau)$ gives lines of spectrum and their widths, whereas eigenvectors $\boldsymbol{B}_\mathrm{k}$ give amplitudes and phases. The matrix $\mathbf{B}_\mathrm{k}$ is derived from the below considerations. Let us assume that the generic eigenvector $|\,\omega_k)$ can be expressed as a linear combination of elements of $\boldsymbol{Q}$. We define:

$$\mathbf{V} = \left[|\,0) \quad |\,1) \quad \ldots \quad |\,M-1)\right] = \left[|\,0) \quad \hat{U}\,|\,0) \quad \ldots \quad \hat{U}^{M-1}\,|\,0)\right] \in \mathbb{C}^{M,M}, \tag{19}$$

as a matrix having the vectors of base $\boldsymbol{Q}$ as its columns, and:

$$\mathbf{B}_k = \begin{bmatrix} B_{k,0} \\ B_{k,1} \\ \\ B_{k,M-1} \end{bmatrix} \in \mathbb{C}^{M,1}, \tag{20}$$

as a vector of appropriate coefficients related to the eigenvectors $|\,\omega_k)$. We can write:

$$|\,\omega_k) = \left[|\,0) \quad |\,1) \quad \ldots \quad |\,M-1)\right] \begin{bmatrix} B_{k,0} \\ B_{k,1} \\ \vdots \\ B_{k,M-1} \end{bmatrix} = \mathbf{V}\mathbf{B}_k. \tag{21}$$

By substituting (21) in the implicit form of (4) the following is obtained:

$$\hat{U}\mathbf{V}\mathbf{B}_k = u_k\mathbf{V}\mathbf{B}_k. \tag{22}$$

By further implicit considerations, pre-multiplying both members by $\mathbf{V}^T$, we obtain:

$$\mathbf{V}^T\hat{U}\mathbf{V}\mathbf{B}_k = \mathbf{V}^T u_k\mathbf{V}\mathbf{B}_k. \tag{23}$$

That leads to (18) which is the generalized eigenvalues problem, where u_k are eigenvalues and $\mathbf{B}_k$ eigenvectors. After solving the problem, having calculated u_k and $\mathbf{B}_k$, the frequencies ω_k are determined by using the following formula:

$$\omega_k = -\frac{1}{\tau}\measuredangle(u_k) = -\frac{1}{\tau}\measuredangle(e^{-j\tau\omega_k}), \tag{24}$$

where τ is a sampling time and a symbol $\measuredangle$ applied to a complex number delivers its phase, *i.e.* $\measuredangle e^{j\vartheta} = \vartheta$. To determine the amplitudes, we employ:

$$d_k = (0\,|\,\omega_k)^2, \tag{25}$$

or, since $|\,\omega_k) = \mathbf{V}\mathbf{B}_k$, after pre-multiplying both members by the vector row $(0\,|$, the previous equation can be also expressed as:

$$(0\,|\,\omega_k) = (0\,|\,\mathbf{V}\mathbf{B}_k. \tag{26}$$

Further on, we obtain:

$$(0\,|\,\omega_k) = (0\,|\left[|\,0) \quad |\,1) \quad \ldots \quad |\,M-1)\right]\mathbf{B}_k. \tag{27}$$

In the aforementioned considerations we have assumed $\mathbf{U}^1, \mathbf{U}^0 \in \mathbb{C}^{M,M}$ symmetric. Based on the previous explanations, now the algorithms should be clear. The software interpreting the algorithm, *i.e.* FFT or STFT, starts with a specific icon where the operator must include essential parameters to start with the acquisition according to (12). The icon is presented in Fig. 5, along with STFT processing. The following parameters are set: type of window (rectangular), sampling rate, window length, step and padding. Flowcharts of FFT and STFT algorithms are shown in Fig. 6.

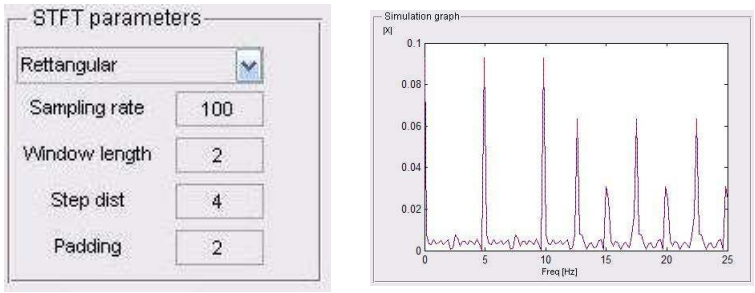

Fig. 5. The set parameters (left) and processed signal according to STFT (right).

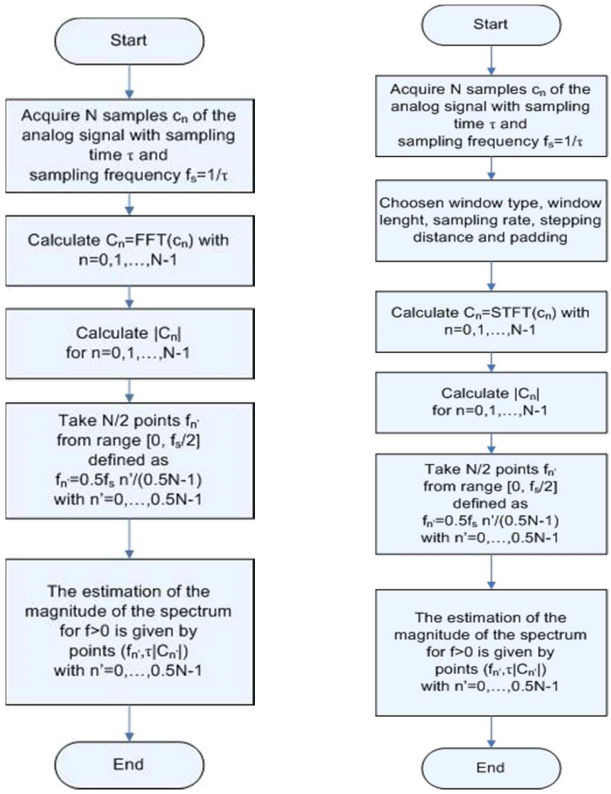

Fig. 6. Flowcharts of the implemented FFT (on the left) and STFT (on the right) algorithms for leak detection.

However, as it will be seen in the results' section, due to intrinsic limitations of FFT and much more those of STFT, we do not obtain better results than we do with FDM, DSD and PDA. That is related to uncertainty values obtained (see 18) with the use of eigenvalues and eigenvectors that are greater than those obtained with other robust techniques. To overcome this key disadvantage, we have implemented, taking inspiration from the Tikhonov regularization method [12], a dedicated algorithm based on an *L*-curve approach [13].

Let us consider a matrix A in the following linear equation:

$$b = Ax + w\,, \tag{28}$$

where: b is a vector of observation; A is a matrix that describes distortion caused by the system under test; x is an unknown object of interest and w is a random vector that represents additional noise. We state that this discrete problem is ill-posed if the following conditions are met:

1. Single values of A gradually decline to zero.
2. The ratio of the greatest single value and the smallest (not null) one is great.

The first condition indicates that in the vicinity there are no problems with a matrix of good-posed coefficients and a well determined numerical rank. The second criterion implies that the matrix is ill-posed, i.e. the solution is sensitive to perturbations. In many cases it happens that matrix A is ill-posed and the main difficulty in ill-posed issues is that they are essentially undetermined because of small single values of A. In the effort to stabilize the problem, adding further information to the desired solution is required: that is the regularization method. It typically requires that a norm 2 of the solution must be small. It is also possible to include an estimation of the solution x_0 in the constraint. The constraint is:

$$\min \Omega(x) \qquad with \;\; \Omega(x) = \left\| L(x - x_0) \right\|. \tag{29}$$

The matrix L can be:

a) Typically, an identity matrix I_n;

b) A discrete approximation $P \times N$ of the derivation operator (n-p) *i-th*.

We define a regularized solution x_q that can minimize the following weighted one of the combination of the residual norm and constraint:

$$x_q = \min_x \left\{ \left\| Ax - b \right\|^2 + q^2 \left\| Lx - x_0 \right\|^2 \right\}, \tag{30}$$

in which $q > 0$ is a regularization parameter:

- for a great q (a great quantity of regularization) a solution agrees with a small norm at the cost of a great residual norm;
- a small q (a small quantity of regularization) has the opposite effect.

Equation 13 can be generalized in the following way:

$$x_q = \arg\min_x \Phi(b, x) + q\Psi(x). \tag{31}$$

A graphical tool more convenient for analysis of discrete ill-posed problems is the so-called L-curve, that means a plot of norm $\left\| Lx_q \right\|$ of a regularized solution in respect to the residual norm $\left\| Ax_q - b \right\|$. In this way, the L-curve clearly demonstrates a compromise between the minimization of both quantities. When q is too great (over-regularization), the curve is essentially a horizontal line. Vice versa, when q is too small (under-regularization), the curve is mainly a vertical line according to Fig. 7 (on the left); q displays a characteristic shape of L. The transition between these two regions, over and under regularization, corresponds to the angle of L-curve, and its relative value of q at this angle (called L-corner) is proposed as the optimum value for q. A flowchart on the right of Fig. 7 shows the algorithm we have implemented to overcome the limitations of using FFT and STFT we recalled before. The algorithm also includes a block of SVD (*Single Value Decomposition*) [14].

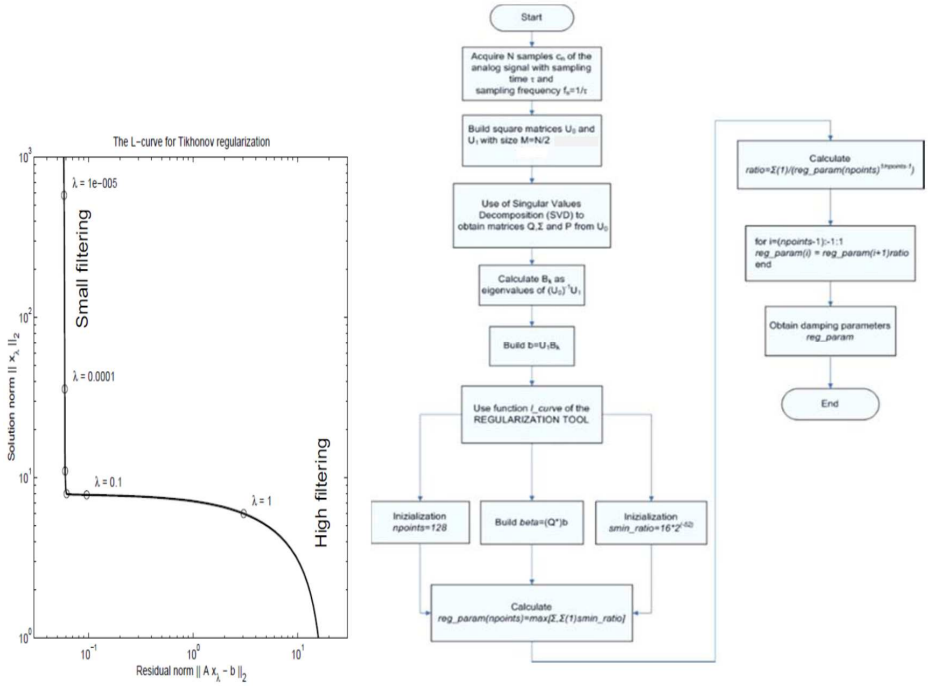

Fig. 7. An *L*-curve for improving the Tikhonov regularization (left) and a flowchart of the proposed algorithm (right).

4. Results and discussion

Before obtaining the values of amplitude, we have performed 5 cycles of tests per water tap, *i.e*. 5 tests for detecting the *j*-th leak with $j = 1,....,11$; an average of all 5 acquired waveforms is as follows:

$$p_j(t) = \frac{1}{5}\sum_{i=1}^{5} p_{i,j}(t)\,. \tag{32}$$

In this way, the obtained signal preserves significant characteristics while the noise is included in the measurements $p_{i,j}(t)$. The explanation of this technical attitude depends upon the fact according to which:

$$p_{i,j}(t) = \overline{p}_{i,j}(t) + n_{i,j}(t), \tag{33}$$

with $\overline{p}_{i,j}(t)$ as a true value of pressure and noise of measurement $n_{i,j}(t)$. The quantity evaluated in $t = t^*$ can be modelled, when i varies, as an aleatory variable with zero average. By considering the 5 variables $n_{i,j}(t^*)$ $i = 1, \ldots, 5$, we obtain:

$$E[n_{i,j}(t^{"})] = \frac{1}{5}\sum_{i=1}^{5} n_{i,j}(t^{"}) \simeq 0\,. \tag{34}$$

The above procedure is repeated for each water tap (valve). At the conclusion of measurements, we have 11 waveforms $p_j(t)$, $j = 1,...,11$, each one describing the behaviour of the system for a given condition of leakage.

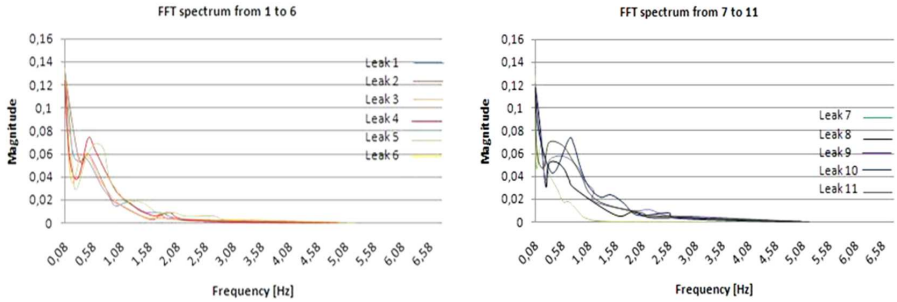

Fig. 8. Different leaks recovered by FFT after single opening of 11 water taps.

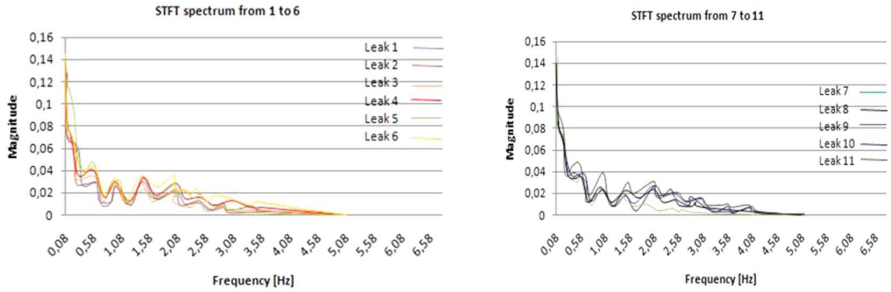

Fig. 9. Different leaks recovered by STFT after single opening of 11 water taps.

Now, we can comment on the results of the previous procedures by applying the algorithms of Fig. 6 that bring the waveforms of Fig. 8 and Fig. 9 for FFT and STFT, respectively. We can see the intrinsic behaviour of both algorithms in the same conditions. Given for instance 1.08 Hz, as we should expect, FFT displays the major peak greater than that of STFT; the same takes place for all useful frequencies. As stated before, we encounter the ill-posed problems that mostly influence the determination of leak locations. The results of Fig. 8 and Fig. 9 must be further treated since the positions of eigenvalues can be located on a circle of radius 1 as depicted in Fig. 10. So our goal is to overcome the ill-posed issue by implementing the algorithm from Fig. 7.

However, it is necessary to notice that the uncertainty is obtained using a specific method for this scope. The data recovered after acquisitions are used for the determination of uncertainty by means of the least mean squares/linear regression. So we should start with the calculation of coefficients of a regression straight line:

$$y = ax + b\,, \tag{35}$$

so that a distance between points is minimal. In (35), we denote x_i expressed in *metres*, and it represents the distance at which we encounter the leak i, with $i = 1,\ldots..,11$, measured from the pressure transducer, whilst y_i is the peak height within the spectrum of Figs. 8 and 9. To retrieve constants of (35), the following formulae are used:

$$b = \frac{\sum_{i=1}^{N} x_i^2 \sum_{i=1}^{N} y_i - \sum_{i=1}^{N} x_i \sum_{i=1}^{N} x_i y_i}{\Delta}\,,$$

$$a = \frac{N\sum_{i=1}^{N} x_i y_i - \sum_{i=1}^{N} x_i \sum_{i=1}^{N} y_i}{\Delta}\,, \tag{36}$$

$$\Delta = N\sum_{i=1}^{N} x_i^2 - \left(\sum_{i=1}^{N} x_i\right)^2,$$

$$\sigma_y = \sqrt{\frac{1}{N}\sum_{i=1}^{N}(y_i - b - ax_i)^2}\,.$$

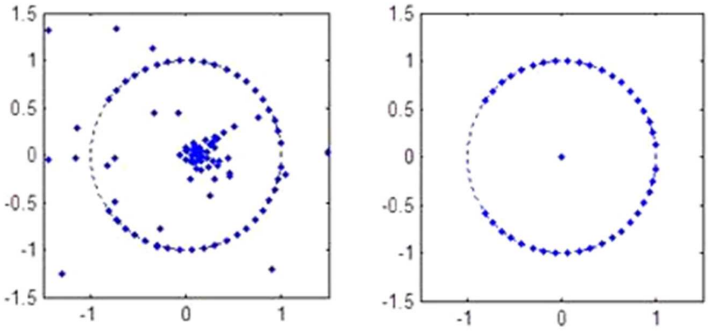

Fig. 10. Locations of eigenvalues before (on the left), and after (on the right) the *L*-curve implementation.

in which a and b are from (35), Δ is a deviation, and σ_y is an uncertainty of amplitude; an uncertainty of distance σ_x is given by the variable x value obtained by reversing (35), *i.e.* $x = \dfrac{y-b}{a}$, and calculating the uncertainty as:

$$\sigma_x = \left[\frac{dx}{dy}\right]\sigma_y = \frac{1}{a}\sigma_y\,. \tag{37}$$

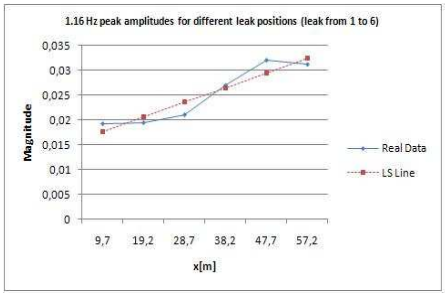

Fig. 11. Interpolation based on the FFT signal of points with peak heights at f =1 Hz taking into account the leak position.

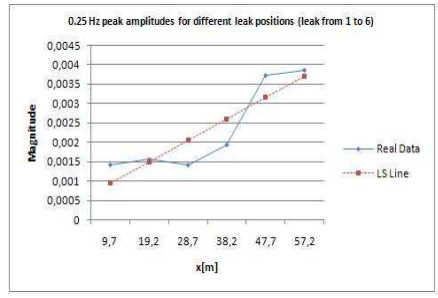

Fig. 12 Interpolation based on the STFT signal of points with peak heights at f = 0.25 Hz taking into account the leak position.

The application of linear regression either FFT or STFT is displayed in Fig. 11 and Fig. 12, at least for the first portion of leaks; LS stands for the least squares method. The plots interpolate the experimental points in a sense of least squares. The final results are shown in Table 1 for FFT and STFT, respectively. For each technique, we present a double result. The first result is related to the use of an *L*-curve that leads to all eigenvalues located on the edge of the circle. The second, instead, reports the implementation of the algorithm without an *L*-curve. As a matter of fact, an *L*-curve gives a great opportunity to reduce the uncertainty. The uncertainty demonstrates the position of leak in respect to the sensor location. It is intuitive to understand that as we move farther from the transducer, the detection of leak location becomes less precise and the uncertainty of it increases.

Table 1. The summarized results of FFT and STFT algorithms.
The improved algorithms are related to eigenvalues located on a circle.

Water tap	Technique	Eigenvalues position	Uncertainty
*R*1 : *R*6	FFT	On circle	±5.20 m
*R*1 : *R*6	FFT	Not fully on circle	±11.52 m
*R*1 : *R*6	STFT	On circle	±7.92 m
*R*1 : *R*6	STFT	Not fully on circle	±12.40 m
*R*7 : *R* 11	FFT	On circle	±5.22 m
*R*7 : *R* 11	FFT	Not fully on circle	±6.90 m
*R*7 : *R* 11	STFT	On circle	±2.60 m
*R*7 : *R* 11	STFT	Not fully on circle	±3.42 m

Certainly, the above results are "worse" in respect with those attained by means of DSD and FDM as reported in references. However, for normal but not complicated waterworks, where we do not generally deal with sudden pressure variations and huge piezo-metric heights, the proposed approach is reliable. For these configurations, the approach is not time-consuming and can offer similar and comparable results.

5. Conclusions

We have presented an enhancement of FFT and STFT techniques for leak detection by applying the *L*-curve approach in accordance with the Tikhonov technique. The Tikhonov regularization is much less numerically expensive than other regularization techniques (as SVD) and reaches its aim of removing the singularity in the denominator, because the new matrix is a Hermitian and positive definite one. FFT is, by definition, the golden standard method of spectral analysis. But, for complex architectures, it displays limitations as well as STFT does. Table I shows comparison of the two algorithms; the improvements are noticed with the implementation of a regularization technique based on an enhanced Tikhonov technique. In general, the FFT algorithm offers better results than the STFT one; but in some circumstances, for specific conditions, STFT can display better results in comparison with FFT. In general, the method of FFT does not provide simple global results for Fourier representations of the input. Such generality and simplicity are usually possible only for linear systems, as for the experimental zig-zag plant of this paper. General results can be obtained for memoryless nonlinearities operating on sinusoidal inputs. This result is not as important as the corresponding result for linear systems because sinusoids are not fundamental building blocks of nonlinear systems, in contrary to the linear ones. This research shows [15] that it is possible to estimate the detection of leaks with good accuracy for zigzag pipelines that have a diameter of less than 20 cm, and we can arrive to around 1 inch as it is done in this paper. These results open opportunities for implementing the algorithm for pipelines used to constitute *e.g.* industrial heat exchangers, or to improve reliability of normal pipelines [16].

References

[1] Kapelan, Z., Savic, D., Walters, G., Covas, D., Graham, N., Maksimovic, C. (2003). An Assessment of the Application of Inverse Transient Analysis for Leak Detection: Part I – Theoretical Considerations. *Computer Control for Water Industry*, London, UK.

[2] Lee, P., Vítkovský, J., Mohapatra, P.K., Chaudhry, M.H., Kassem, A.A., Moloo, J. (2006). Detection of Partial Blockage in Single Pipelines. *Journal of Hydraulic Engineering*, ASCE, 132(2), 200–206.

[3] Lay-Ekuakille, A., Vendramin, G., Trotta, A. (2009). Spectral Analysis of Leak Detection in a Zigzag Pipeline: A Filter Diagonalization Method – based algorithm application. *Measurement*, 42(3), 358–367.

[4] Lay-Ekuakille, A., Vendramin, G., Trotta, A. (2010). Robust Spectral Leak Detection of Complex Pipelines using Filter Diagonalization Method. *IEEE Sensors Journal*, 9(11), 1605–1614.

[5] Lay-Ekuakille, A., Vergallo, P. (2014). Decimated Signal Diagonalization Method for Improved Spectral Leak Detection in Pipelines. *IEEE Sensors Journal*, 14(6), 1741–1748.

[6] Lay-Ekuakille, A., Vergallo, P., Griffo, G. (2013). A Robust Algorithm based on Decimated Padé Approximant Technique for Processing Sensor Data in Leak detection in Waterworks. *IET Science, Measurement & Technology*, 7(5), 256–264.

[7] Griffin, D.W., Lim, J.S. (1984). Signal estimation from modified short-time Fourier transform. *IEEE Trans. Acoustics, Speech, and Signal Proc.*, 32(2), 236–243.

[8] Lay-Ekuakille, A., Vendramin, G,, Trotta, A., Vanderbemdem, P. (2009). STFT-based spectral analysis of urban waterworks leakage detection. *XIX IMEKO World Congress Proc.*, Lisbon, Portugal.

[9] Liou, C.P., Tian, J. (1995). Leak Detection – A Transient Flow Simulation Approach. *Journal of Energy Resources Technology, American Society of Mechanical Engineers*, 117(3), 243–248.

[10] Nash, G.A., Karney B.W. (1999), Efficient Inverse Transient Analysis in Series Pipe Systems. J*ournal of Hydraulic Engineering*, 125(7), 761–764.

[11] Lay-Ekuakille, A., Pariset, C., Trotta, A. (2010). FDM-based Leak Detection of Complex Pipelines: Robust Technique for Eigenvalues Assessment. *Measurements Science Technology*, 21, 1–10.

[12] Walkins, D.S. (2007). *The matrix Eigen Problem*. SIAM, 351–421.

[13] Calvetti, D., *et al.* (2000). Tikhonov regularization and the L-curve for large discrete ill-posed problems. *Journal of Computational and Applied Mathematics*, 123(1–2), 423–446.

[14] Hansen, P.C. (1998). *Rank-Deficient and Discrete Ill-posed Problems*. Siam, Philadelphia, USA.

[15] Lay-Ekuakille, A., Vergallo, P., Trotta, A. (2010). Impedance Method for Urban Waterworks: Experimental Frequency Analysis for Leakage Detection. *Imeko Tc-4, TC-19 and IWADC Conference*, Kosice, Slovakia.

[16] Ozevin, D., Yalcinkaya, H. (2014). New Leak Localization Approach in Pipelines Using Single-Point Measurement. *Journal of Pipeline Systems Engineering and Practice*, 5(2), 1–8.